New Concepts and Perspectives on Micro-Rotorcraft and Small Autonomous Rotary-Wing Vehicles

L.A. Young
E.W. Aiken
Army/NASA Rotorcraft Division
NASA Ames Research Center
Moffett Field, CA 94035

J.L. Johnson
Aerospace Computing, Inc.
Los Gatos, CA

R. Demblewski
College of San Mateo

J. Andrews
Massachusetts Institute of Technology
NASA Education Associates Program

J. Klem
San Jose State University

Abstract

This paper summarizes ongoing work concerning micro-rotorcraft (MRC) – i.e., rotary-wing micro air vehicles (MAV) – research and development. Technology trends involving microelectronic miniaturization, vehicle autonomy systems, electric propulsion and power electronics are contributing to an ongoing revolution in MAV and MRC aerial vehicle concepts and applications. New vehicle configurations are being developed, as well as old concepts being reassessed, for MAV and MRC vehicles.

Nomenclature

a	Speed of sound, m/sec
A	Rotor disk area, $A=\pi R^2$, m^2
c_{do}	Rotor blade airfoil mean profile drag coefficient
$C_{L\alpha}$	Rotor blade airfoil mean lift curve slope
C_L	Sectional airfoil lift coefficient
C_P	Power Coefficient, $C_P = P/\rho A V_{Tip}^3$
C_T	Thrust Coefficient, $C_T = T/\rho A V_{Tip}^2$
c_{Ref}	Blade reference chord length, c_{Ref}= S/R, m
c_{Tip}	Blade tip chord length, m
FM	Rotor Figure of Merit
k	Rotor induced power constant
M_{Tip}	Tip Mach number
N	Number of rotor blades per rotor
P	Rotor power, Watt
Q	Rotor shaft torque, N-m, $Q=P/\Omega$
R	Rotor radius, m
r_c	Nondimensional blade-root cut-out (fraction of R)
Re_{Tip}	Tip Reynolds number
S	(Single) blade planform area, m^2
T	Rotor thrust, N
V_{Tip}	Tip speed, m/sec, $V_{Tip} = \Omega R$
AR	Rotor blade aspect ratio, $AR=R^2/S$
α	Sectional airfoil angle of attack, deg.
α_0	Airfoil mean zero-lift angle-of-attack, deg.
η_{em}	Motor/drive-train electromechanical efficiency
ρ	Atmospheric density
σ	Rotor solidity, $\sigma = Nc_{Ref}/\pi R$
$\theta_{0.75}$	Rotor collective, blade pitch angle at 75% radius
θ_{tw}	Linear twist rate of blades, Deg.
Ω	Rotor speed, radians/sec

Presented at the 20th AIAA Applied Aerodynamics Conference, St. Louis, MO, June 24-27, 2002.

Introduction

A research effort is currently underway at NASA Ames Research Center studying the enabling technologies for small autonomous rotorcraft (Ref. 1). Small autonomous rotorcraft are defined for the purposes of this paper to be a class of vehicles that ranges in size from rotary-wing micro air vehicles (MAVs) to larger, more conventionally sized,

rotorcraft uninhabited aerial vehicles (UAVs) – i.e., vehicle gross weights ranging from hundreds of grams to thousands of kilograms.

Small autonomous rotorcraft represent both a technology challenge and a potential new vehicle class that may have substantial societal impact. Rotary-wing micro air vehicles are referred to in this paper as "micro-rotorcraft" (MRC).

The technical discussion within this paper focuses on three areas: concept development of MRC through prototyping, hover performance and aerodynamic measurements of MRC-representative rotors, and an assessment of preliminary design weight trend information applicable for MRC.

Design and Technology Effort

Several micro-rotorcraft projects have been previously reported in the literature (Refs. 2, 3, and 4, for example). There are two technical approaches to micro-rotorcraft research efforts: emphasizing the miniaturization challenges of the micro-rotorcraft, or, alternatively, focusing on advanced vehicle design and aerodynamic challenges of MRC. The work reported in this paper focuses on the latter technical approach. Further, the work at NASA Ames has focused on the usage of electric propulsion for micro-rotorcraft proof-of-concept vehicles.

A number of micro-rotorcraft concepts have been taken to an initial proof-of-concept test article stage. These vehicles and their associated proof-of-concept testing will be briefly discussed next.

Quad-Rotor Tail-Sitter

Figure 1 is a photograph of a quad-rotor tail-sitter concept. Quad-rotor designs employing rotor speed control for vehicle trim yields a very simple but very effective control system approach. The simplicity of rotor speed control lends itself well to micro-rotorcraft applications where sub-system packaging, and providing control power for very small vehicles, becomes extremely difficult. Combining a flying-wing, tail-sitter design with quad-rotor propulsion and trim control potentially results in a vehicle that has full hover capability but with high-speed aerodynamic efficiency, that would have significant improvements in range and endurance over other MRC concepts. Employing a flying wing in the design also allows for the possible integration of solar-cell arrays on the wing surface, and thereby enabling long-term, extended duration missions. The limited wing area available in a small vehicle would dictate that it would have to recharge on the ground, between flights, but would allow several flights over several days, at several different surveillance sites.

Fig. 1 – Quad-Rotor Tail-sitter in Hover Mode

Tail-sitter designs have had a mixed history. However, many developmental problems and limitations were a consequence of the flight demonstrators being inhabited/piloted aircraft. UAV applications for tail-sitter designs would likely be perfectly acceptable vehicle configurations.

Controlled hover and low-speed flight has been successfully demonstrated to date for the quad-rotor tail-sitter. Forward-flight transition has also been demonstrated; further vehicle improvements are required before demonstrating sustained controlled forward-flight.

'Mini-Morpher'

Micro-rotorcraft missions will likely require these vehicles to fly at low-altitudes, in the close presence of people and buildings. Such close proximity with objects and people to potentially collide with will dictate micro-rotorcraft to have as small a mass and impact momentum as possible, while still meeting overall mission requirements. Further, this same concern regarding low-altitude collision with people and objects will foster the development of vehicles that in some manner embody design features to physically protect their rotors and other critical hardware from casual impact damage. This is why there is considerable recent interest in ducted-fan versions of vertical lift micro air vehicles.

Recent improvements in active flight controls and smart materials/actuators now make possible low-mass micro-mechanical systems that allow micro-rotorcraft designs that can "morph," i.e., change vehicle geometry to match flight condition.

A number of concepts have been developed at NASA Ames related to using morphing vehicle technology to "shroud" micro-rotorcraft rotors while in hover and low-speed flight, and then to change configuration in high-speed forward flight to maximize aerodynamic efficiency. One such concept is the "mini-morpher" – see Fig. 2.

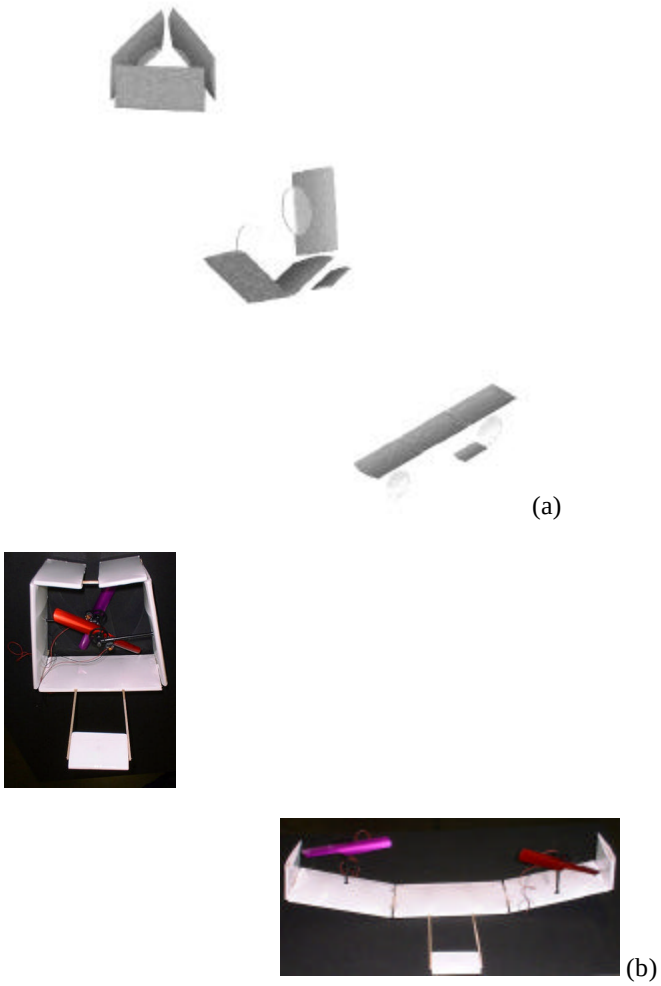

(a)

(b)

Fig. 2 -- 'Mini-Morpher' Transitioning from Hover (Top Left) to Forward-Flight (Bottom Right): (a) Concept and (b) Prototype/Test Article

Only tethered hover testing has been demonstrated to date with the mini-morpher test articles (Fig. 3). The rotor diameter for the mini-morpher coaxial rotors is quite small – a radius of 0.08 m. Two low aspect ratio, high solidity rotors (σ=0.3) have been used in the prototype vehicle.

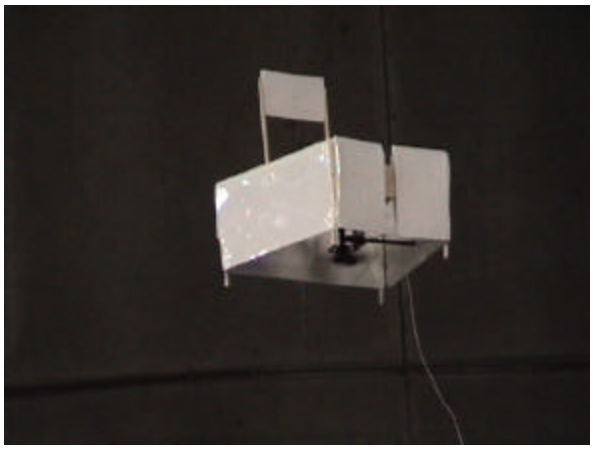

Fig. 3 -- Mini-Morpher In-flight in Hover

Figure 4 shows representative isolated rotor performance data for the mini-morpher vehicle. The rotor has fixed-pitch blades; thrust can only be varied by speed control.

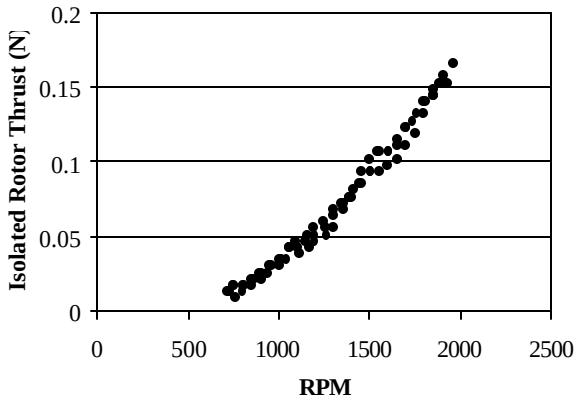

Fig. 4 – Mini-Morpher Isolated Rotor Thrust as a function of RPM

Details as to the methodology for the rotor hover performance measurements made for individual MRC concepts, and low Reynolds number rotors in general, will be discussed later in the paper.

Tandem Twin-Fuselage Tiltrotor

The pursuit of efficient forward flight characteristics while preserving good hover performance is the goal for all rotary-wing vehicles. However, to pursue this goal while at the same time examining means by which to minimize overall

vehicle size and the potential for low-altitude (from ground level to a couple hundred feet at most) collision damage to the vehicle and people/surroundings makes for a unique design challenge.

The conventional tiltrotor aircraft configuration meets the prerequisite requirements for efficient hover and forward-flight. However, because the tiltrotor aircraft's rotor and engine nacelles are mounted at the vehicle's wing-tips, micro-rotorcraft versions of these vehicles would be especially prone to low-altitude collision damage with people and objects (as well as from landing on rough ground/vegetation). An alternate tiltrotor/tilt-wing configuration is currently being considered at Ames: a twin-fuselage, tandem tiltrotor (Fig. 5). The twin fuselages of this vehicle protects its rotors from accidental impact/collision damage by nestling the rotors between the fuselage airframes.

(a)

(b)

Fig. 5 – Tandem Twin-Fuselage Tiltrotor: (a) Concept and (b) Prototype

Figure 6 shows representative three-bladed isolated rotor hover data for one of the rotors employed on the tandem tiltrotor proof-of-concept vehicle. This rotor is 0.458m diameter, has a solidity of 0.095, is flat-pitch in twist, and employs symmetrical conventional airfoils that are 12.5% thick. This rotor is not an optimized proprotor design for hover and forward flight. Hobbyist components are useful for quick, low-cost prototyping of vehicle concepts.

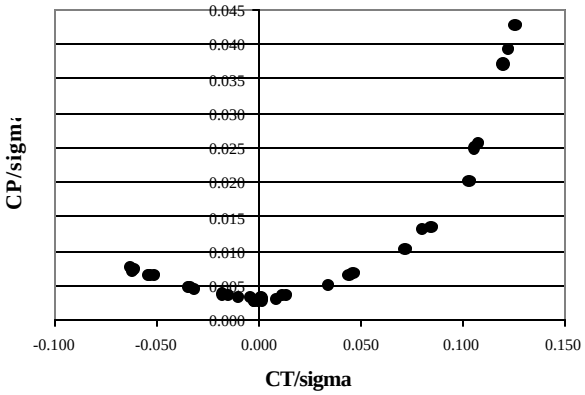

(a)

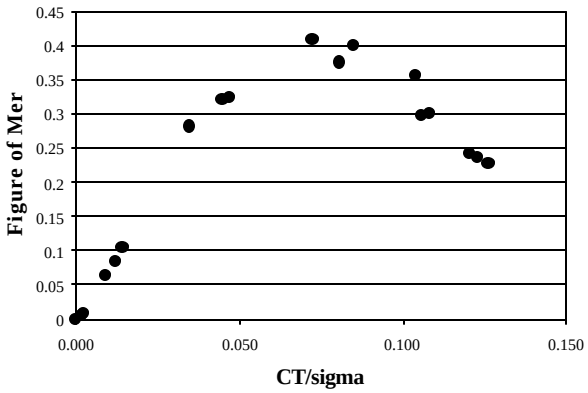

(b)

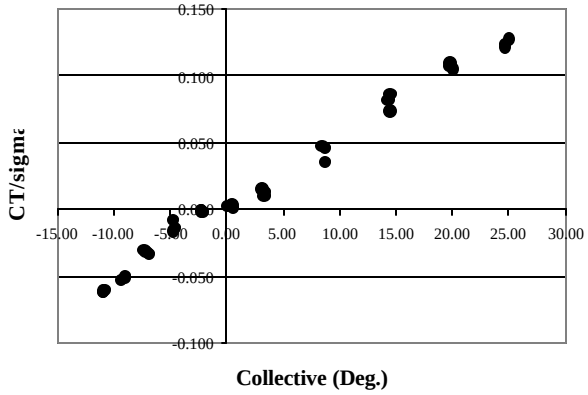

(c)

Fig. 6 – 'Tandem Tiltrotor' Three-Bladed Rotor (a) CP versus CT, (b) Figure of Merit, and (c) CT versus collective

Coaxial Helicopter

Coaxial helicopters have been a reality for several decades now – including a series of UAV or RPV platforms (the Candair CL-237, the Westland 'Sprite,' and the Gyrodyne

QH-50, among others). Even a few custom-built coaxial hobbyist RC models have been flown. These coaxial helicopter UAVs are fairly complex mechanical systems and their implementation becomes ever increasingly difficult as the scale of the vehicle is reduced to very small sizes.

An alternate approach is being studied (Fig. 7). By employing two fully symmetric (but mirrored) drive trains, control systems, and rotors, a simple coaxial helicopter configuration has been developed. A graphite composite structure incorporating a cross-braces, sponsons or cross-arms, and landing gear supports the two independent drive trains. Vehicle yaw control is effected by differential torque from the two drive trains, resulting from a differential collective setting for the two rotors.

(a)

(b)

Fig. 7 – Coaxial Helicopter: (a) Concept and (b) Prototype

The coaxial helicopter rotor blades are untwisted (flat pitch) and the blade airfoils are symmetrical. Each rotor is two-bladed with a teetering hub and a Bell-Hiller flybar (with paddles) design. The rotor control systems are mechanically coupled together and can provide both differential collective and cyclic control. A 16-cell lithium-ion battery pack yields approximately 6 minutes of typical hover and low-speed loiter flight time (Fig. 8). The rotor diameter is 0.982 meters and the gross weight is 3.5 kg.

Fig. 8 – MRC Coaxial Helicopter Take-off on First Flight

The intent of the research at NASA Ames is not to identify the 'best' micro-rotorcraft design, from a field of prospective candidates. Instead, the objective of the work is to suggest that considerable opportunities exist to think 'outside the box' and consider wholly new vehicle configurations for micro-rotorcraft and other small autonomous rotary-wing vehicles. It would be extremely disappointing – and ultimately self-defeating -- if only very small versions of existing, conventional inhabited/piloted rotorcraft types were developed for micro-rotorcraft applications.

General Micro-Rotorcraft Hover Performance Characteristics

Rotor performance is a crucial aspect of micro-rotorcraft and small autonomous rotary-wing vehicles. In addition to the inhouse work at NASA Ames focusing on vehicle concept development, a complementary effort is being conducted examining rotor aerodynamics for very small rotor systems. These hover experiments were conducted with fairly simple test apparatus (Fig. 9). The results from this series of low Reynolds number rotor tests for hover performance for a variety of rotor configurations of the approximate scale of micro-rotorcraft vehicles will next be discussed.

Experimental Description

To perform hover tests of small, low Reynolds rotors, a lever arm scale system was constructed. The lever arm apparatus was designed in the shape of a sideways "T" (Fig. 9).

Fig. 9 -- MRC Hover Test Stand

The vertical support for the test stand was designed with sufficient height to keep the rotor out of ground effect. The test stand vertical support was attached to a "balance arm" that was pivoted. A lever ratio -- that was a function of the relative distance of the rotor axis to the pivot, versus the distance from the pivot to a knife-edge resting on a digital scale – created a means by which the scale sensitivity with respect to rotor thrust could be adjusted. Rotors of various blade shapes were installed on the test stand and spun at several different rotor speeds. RPM was varied remotely by a radio transmitter. Rotor speed was measured by a digital tachometer. Rotor thrust was measured by a digital scale, which rested under one end of the test stand lever arms. A simple lever ratio was used to calculate the actual thrust output of the rotor from the digital scale. Input power for the test stand motor was recorded by use of a wattmeter attached to the power input cables. Rotor shaft power was estimated using a correction methodology based on electric motor/drive-train efficiency estimates determined through rotor bat (Ref. 5) and Prony brake measurements (refer to the Appendix).

Hobbyist radio-controlled (RC) helicopter model aluminum rotor blades were utilized for these experiments. The blades were tested in one of two configurations: a tapered blade set, and a rectangular (constant chord) blade set. Figure 10 shows some of the rotor blades tested.

Fig. 10 -- Tapered Blades

All of the rotors tested (with the exception of the mini-morpher and tandem tiltrotor rotors) had flat plate airfoils with circular arc camber. The radius of the circular arc is constant for all tapered and rectangular planform blade sets. Both the airfoil percent camber (maximum camber line displacement located at the airfoil 50% chordwise station) and the blade twist distribution are approximately linear (for example, Fig. 11). The twist and camber of the tested low Reynolds number tapered blade rotors are relatively high compared to conventional helicopter airfoils. The airfoil flat-plate thickness is 0.4 mm. The rectangular blade rotors have zero twist rate and constant camber.

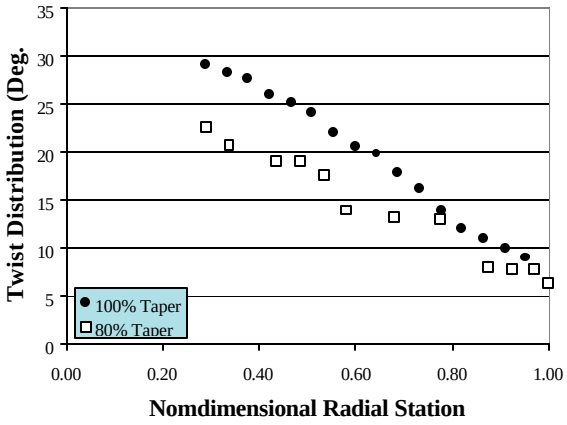

(a)

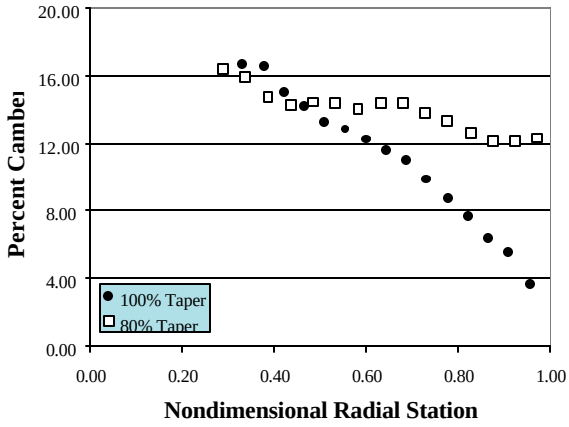

(b)

Fig. 11 – Tapered Blade (a) Twist and (b) Camber

Table 1 is a brief summary of the rotors tested. Only two-bladed rotors were tested – with the exception of the three-bladed tandem tiltrotor rotor and a three-bladed rotor that uses the same blades as the two-bladed "100% tapered blade" configuration. The "percent" designation for the tapered blade rotors refers to the percent planform blade area of the rotor with respect to the 'baseline' rotor for a given general configuration. The "percent" designation for the

rectangular blade rotor is in reference to the percent solidity with respect to the baseline rectangular rotor.

Table 1 – Rotor Descriptions

Rotor Identification	R (m)	c_{Tip} (m)	S (m^2)	σ	*AR*	Taper
"100%" Unmodified Tapered Blade (Rounded Tip)[a]	0.286	0.023	0.0081	0.063	10.1	0.541
100% (Planform Area) Modified Blade (Square Tip)	0.280	0.023	0.0079	0.064	9.9	0.537
95% Tapered Blade	0.281	0.021	0.0077	0.062	10.3	0.504
90% Tapered Blade	0.275	0.020	0.0072	0.061	10.5	0.476
85% Tapered Blade	0.268	0.020	0.0070	0.062	10.3	0.488
80% Tapered Blade	0.260	0.019	0.0065	0.061	10.4	0.468
75% Tapered Blade	0.253	0.018	0.0061	0.061	10.5	0.453
60% Tapered Blade	0.245	0.015	0.0051	0.054	11.9	0.453
80%(Solidity) Rectangular Blades	0.259	0.023	0.0050	0.055	11.5	1.0
90% Rectangular	0.235	0.023	0.0044	0.061	10.2	1.0
100% Rectangular	0.215	0.023	0.0040	0.067	9.6	1.0
Mini-Morpher	0.08	0.020	0.0031	0.308	2.1	0.920
3-Bladed 100% Tapered Rotor[a]	0.286	0.023	0.0081	0.095	10.1	0.541
Three-bladed Tandem Tiltrotor	0.458	0.044	0.0202	0.092	10.4	1.0

[a]Identical blades used between the two rotors (two- and three-bladed); cambered, circular arc airfoils.

The tapered blades were tested at 1000, 900, and 800 RPM to acquire a performance database for this type of rotor. Each set was also tested at a nominal RPM that resulted in a blade tip Mach number of approximately 0.07. Tip Reynolds numbers ranged from approximately 39,000 to 25,700.

Three rectangular blade sets were fabricated to test the effect of changes in solidity and blade aspect ratio on low Reynolds number rotors. These blades were manufactured from the same aluminum blades as before, but were modified to a rectangular shape. A constant chord of 2.25 cm was maintained while the length of the blade was shortened to vary rotor solidity and blade aspect ratio. Testing was also conducted with the rectangular blade sets at 1000, 900, 800, and a nominal RPM to match a tip Mach of 0.07. Since the blade chord was identical with each rectangular planform blade set, it was possible to match tip Reynolds number along with tip Mach.

The rotors were tested over a range of blade pitch angles (rotor collective) that varied from approximately -10 to +18 degrees, as measured at the 75% blade radial station. Multiple runs were conducted for each rotor to assess data repeatability.

Hub tares were subtracted out of the rotor data for each separate RPM tested. Also, it was determined from rotor bat and Prony brake tests that motor efficiency was approximately constant in the 800 to 1100 RPM range, as well as independent of torque loading for loads greater than 0.3 N-m (refer to the Appendix). From the rotor bat and Prony brake data a correction/estimation methodology was developed to derive estimates of rotor shaft power from motor input power measurements.

Experimental Results

Tapered Blades

Figure 12 data shows large Reynolds number effects on rotor performance. All tapered blade rotors in Fig. 12 are tested at a tip Mach number of 0.07. The tip Reynolds numbers range from 26,000 to 35,000, depending on blade taper. Maximum figure of merit for the low Reynolds number rotors range from 0.35 to 0.53. Regression analysis of the thrust and power data set yield estimates of the mean airfoil profile drag coefficient, c_{d0}, generally within the range of 0.07 to 0.12. These rotor data derived mean profile drag coefficients are higher than comparable two-dimensional cambered circular arc airfoil drag coefficients, which are on the order of 0.03 to 0.05 (Ref. 6). Estimates of induced power constant, k, derived from regression analysis of the performance data, ranged generally from 1.1 to 1.4. Most estimates of the induced power constant were approximately k=1.2, which is fairly representative of induced power constants seen for large, conventional helicopter rotors. In addition to Reynolds number effects, the geometry of the tapered blade rotors, with cambered circular arc flat plate airfoils, manifests small variations in twist and camber distributions with changes in taper ratio (Fig. 11).

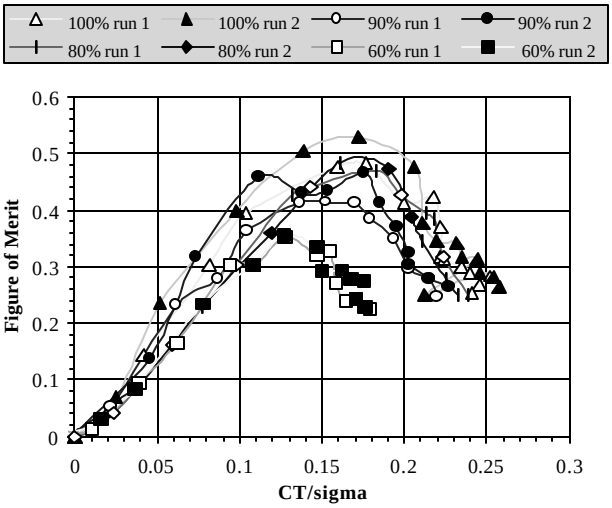

Fig. 12 – Tapered Blade Rotor Figure of Merit Curves (M_{Tip}=0.07)

Figure 13 shows the C_P/σ versus C_T/σ curve for the same tip Mach number, once again increasing rotor thrust by increasing collective. The general trend of the thrust power polar curve is similar to large conventional rotorcraft.

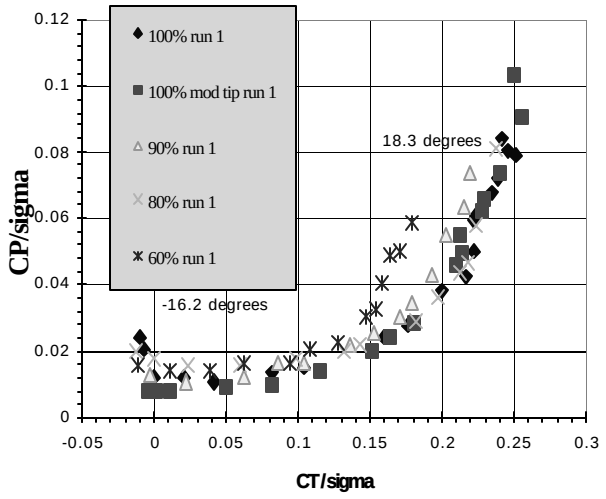

Fig. 13 – Tapered Blade Rotor Thrust and Power Polar (M_{Tip}=0.07)

The C_T/σ versus collective curves are shown in Fig. 14. This near linear trend of thrust coefficient with collective is also similar to that found for larger rotorcraft. The onset of blade stall occurs at about 8-10 degree collective.

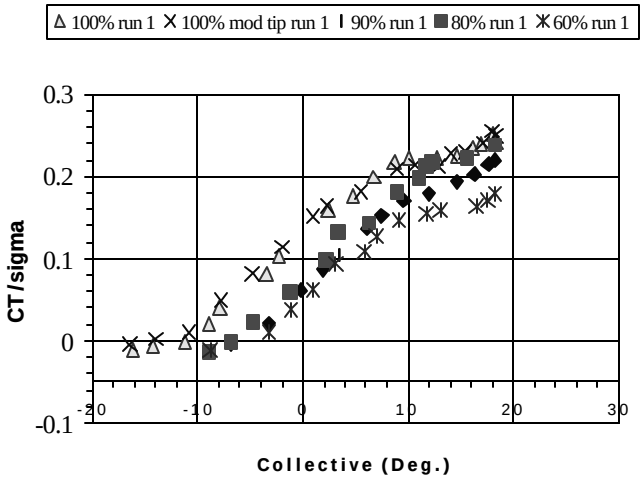

Fig. 14 – Tapered Blade Rotor Thrust Coefficient versus Collective (M_{Tip}=0.07)

As an interesting aside, a comparison was made between a two-bladed rotor ("100% Tapered") and a three-bladed tapered rotor. Both rotors used the same rotor blades with the same cambered circular arc airfoils. The solidity for these rotors is 0.063 and 0.095, respectively. There is very little discernable difference in rotor performance between the two rotors, despite the differences in solidity and blade count (Fig. 15).

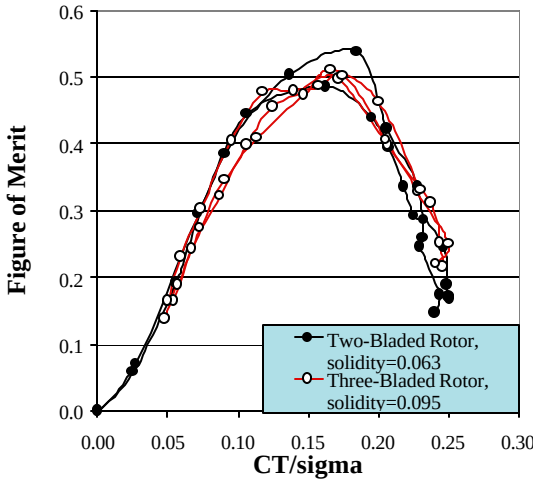

Fig. 15 – Two versus Three-Bladed Rotor Performance (Re_{Tip}=47,000 and 1000 RPM)

Rectangular Blades

Hover performance curves for the rectangular blade sets will now be discussed. The figure of merit curves are shown in Fig. 16. The C_P/σ versus C_T/σ curves are shown in Fig. 17. The thrust coefficient versus collective curves are shown in Fig. 18. In all three figures, the tip Mach and tip Reynolds numbers are kept constant at M_{Tip}=0.067 and Re_{Tip}=35,000. The maximum figure of merit for the three rectangular blade rotors ranges from 0.34 to 0.52, very similar to the tapered blade rotor data set. Estimates of mean airfoil profile drag coefficients for the three rotors (based on least-squares regression analysis) range from 0.06 to 0.12, again in general agreement with the tapered blade rotor results. Induced power constant estimates, k, from regression analysis of the thrust and power data for the three rectangular blade rotors are all within the range of 1.16 to 1.2 – thereby demonstrating less variability in magnitude than the tapered blade rotor estimates.

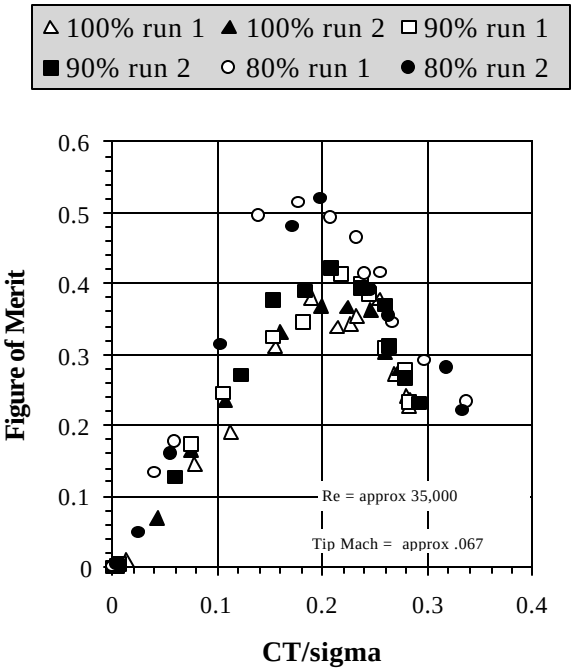

Fig. 16 – Rectangular Blade Rotor Figure of Merit Curves

Fig. 16 results show the effect of rotor solidity and/or blade aspect ratio on rotor hover performance, for these very small low Reynolds number rotors. The general trends for the rectangular (constant chord) blade rotors' thrust and power polar (Fig. 17) and the thrust/collective curves (Fig. 18) are similar to the tapered blade rotor results.

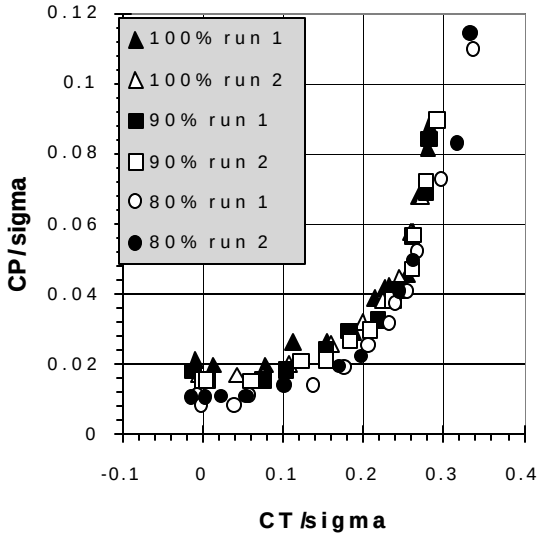

Fig. 17 —Thrust and Power Polar for Rectangular Blade MRC Rotors

It is noteworthy to point out that the onset of blade stall can be seen in Fig. 18, which is even more pronounced for the rectangular blades than the tapered blades. Again, blade stall occurs at approximately 10 degrees collective. Estimates of the mean airfoil lift curve slope, derived from least-squares regression analysis of the thrust and collective data set, range from 4.6 to 5.3/radians. This significantly lower than often-cited nominal mean lift curve slope values (~5.7/radians) for conventional helicopter rotors (Ref. 7). Because of the large blade airfoil camber, the collective angle at which zero thrust is achieved for the three rectangular blade rotors is approximately –5 degrees.

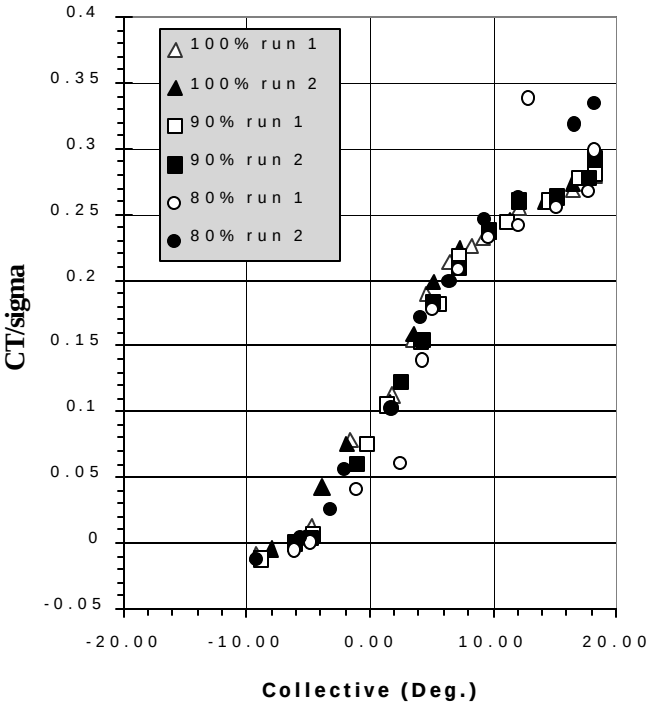

Fig. 18 – Rectangular Blade Rotor Thrust Coefficient versus Collective

Micro-Rotorcraft Weight Trends

Existing rotorcraft preliminary design (PD) tools are incompatible with micro-rotorcraft applications. In particular, weight trend data and PD weight equations are not scaleable to these very small vehicle sizes. What the rotorcraft community requires is a set of PD tools that is broadly applicable across the spectrum of rotary-wing vehicles -- including not only conventional (inhabited) rotorcraft but rotorcraft UAVs, small autonomous rotary-wing vehicles, and micro-rotorcraft. As an incremental step

towards developing such cross-spectrum design tools, a database of RC hobbyist model component weights (fixed- and rotary-wing) is being developed for a variety of vehicles. This information will be used to develop extensions to rotorcraft preliminary design weight equations so as to be applicable to MRC. The original functional form of these equations will be derived from standard rotorcraft PD weight equations (see Refs. 8-12), but are being empirically calibrated to the smaller vehicle weight trend data (Table 2 and Figs. 19 and 20). The radio-controlled electric helicopter weight data is being used as MRC analogs in this engineering context. These modified PD weight equations will also be refined to accommodate predictions of rotary-wing hardware for vertical lift planetary aerial vehicles (Ref. 13, for example).

Table 2 – RC Electric Helicopter Weight Data (In Terms of Percent Gross Weight for Three Vehicle Sizes)

	% GW		
	0.3 kg	**1.8 kg**	**3.7 kg**
Rotor System	11.0	11.2	13.9
Tailboom Assembly	8.0	9.1	7.8
Main Rotor Motor (Electric)	15.4	10.5	8.1
Fuselage/Structure	7.0	15.1	12.0
Main Transmission	2.0	3.4	3.4
Landing Gear	2.3	3.4	2.9
Control System	5.7	18.3	9.3
Flight Control Avionics & Teleoperation System	29.4	2.4	1.6
Power Source (battery)	19.2	26.6	41.0

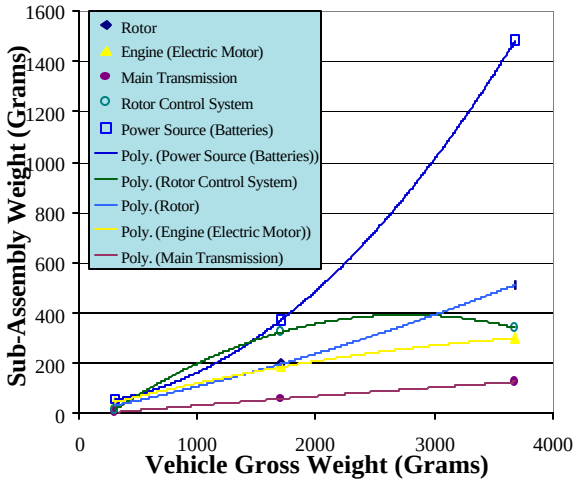

Fig. 19 – Rotor/Propulsion System Weights

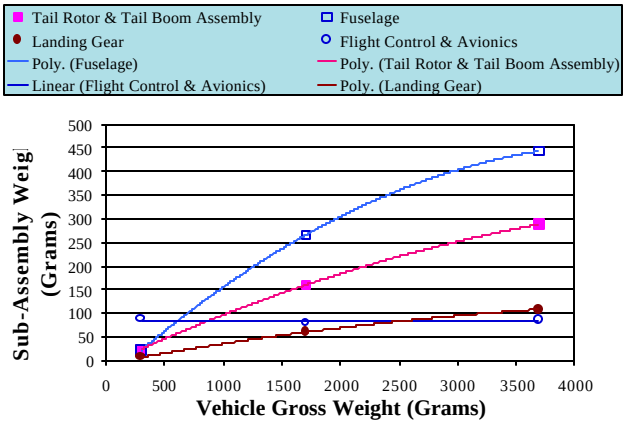

Fig.20 – Airframe Component Weights

Future Work

Work continues developing and refining new vehicle concepts for micro-rotorcraft applications. As concepts are matured beyond the proof-of-concept phase then issues of automated flight control will be examined and implemented from a research perspective. The ultimate goal of the micro-rotorcraft project is the development of a suite of concepts and technologies that will enable a new class of flight vehicles to enter into practical application.

One of the side benefits of the NASA Ames micro-rotorcraft project is the opportunity to propose and examine innovative vehicle concepts that could not be cost-effectively evaluated at larger scales. Ultimately, a set of vehicle concepts and design tools that address a broad range of vehicle weight classes – from hundreds of grams to thousands of kilograms – will benefit from the work reported in this paper.

Concluding Remarks

Three noteworthy accomplishments have been made and reported in this paper as related to the development and understanding of micro-rotorcraft and small autonomous rotary-wing vehicles: 1. A series of innovative vehicle concepts suitable for application to micro-rotorcraft and small autonomous rotorcraft have been proposed and studied with respect to establishing initial proof-of-concept; 2. A general assessment of the hover performance characteristics of low Reynolds rotors has been experimentally evaluated; 3. Weight trend information has begun to be collected that will aid in bridging the gap between preliminary design tools

for conventional rotary-wing flight vehicles and micro-rotorcraft. The results of this paper will hopefully inspire follow-on work to fully realize the potential benefits of micro-rotorcraft and small autonomous rotary-wing vehicles for our society.

Acknowledgement

The work summarized in this paper was supported by discretionary funding from the Aerospace Directorate at NASA Ames Research Center. Finally, the technical contributions of Ms. Naomi Tsafnat to the Ames micro-rotorcraft project is gratefully acknowledged.

References

1. Aiken, E.W., Ormiston, R.A., and Young, L.A., "Future Directions in Rotorcraft Technology at Ames Research Center," 56th Annual Forum of the American Helicopter Society, International, Virginia Beach, VA, May 24, 2000.

2. Kroo, I., "Whirlybugs," New Scientist, June 5, 1999.

3. Kroo, I. and Kunz, P., "Development of the Mesicopter: A Miniature Autonomous Rotorcraft," American Helicopter Society (AHS) Vertical Lift Aircraft Design Conference, San Francisco, CA, January 2000.

4. Samuals, P., et al, "MICOR," AHS Vertical Lift Aircraft Design Conference, San Francisco, CA, January 2000.

5. Harris, F.D., "Power Required by Whirling Pipes at μ=0," NASA TM (To be Published).

6. Hoerner, S.F. and Borst, H.V., Fluid-Dynamic Lift, Hoerner Fluid Dynamics, Brick Town, NJ, pg. 2-17,1985.

7. Johnson, W.R., *Helicopter Theory*, Princeton University Press, 1980.

8. Davis, A.J. and Wisniewski, J.S., "User's Manual for HESCOMP: The Helicopter Sizing and Performance Computer Program," NASA CR 152018, September 1973.

9. Stepniewski, W.Z. and Shinn, R.A., "Soviet Vs. U.S. Helicopter Weight Prediction Methods," 39th Annual Forum of the American Helicopter Society, St. Louis, MO, May 9-11, 1983.

10. Stepniewski, W.Z., "Some Weight Aspects of Soviet Helicopters," 40th Annual Forum of the American Helicopter Society, Arlington, VA, May 16-18, 1984.

11. Vega, E., "Advanced Technology Impacts on Rotorcraft Weight," 40th Annual Forum of the American Helicopter Society, Arlington, VA, May 16-18, 1984.

12. Smith, H.G., "Helicopter Structural Weight Prediction and Evaluation – Theory Versus Statistics," 26th Annual Forum of the American Helicopter Society, Washington, DC, June 16-18, 1970.

13. Young, L.A., Aiken, E.W., Derby, M.R., Navarrete, J., and Demblewski, R., "Experimental Investigation and Demonstration of Rotary-Wing Technologies for Flight in the Atmosphere of Mars," 58th Annual Forum of the AHS, International, Montreal, Canada, June 11-13, 2002.

Appendix – Deriving Rotor Shaft Power

The MRC hover test stand motor input power was directly measured by means of a digital wattmeter. In order to derive estimates of rotor shaft output power the motor/drive-train efficiency had to be estimated for a given operating condition (speed and torque load). The methodology for deriving the rotor shaft output power is discussed in this appendix.

Two independent approaches were taken to derive motor/drive-train efficiency estimates for the MRC hover test stand: use of "rotor bat" data and acquisition of Prony brake data for the MRC test-stand. Both approaches yielded comparable results, and, ultimately, both sets of data were compiled together to derive the correction methodology used for the MRC hover testing.

Figure 21 shows the bat test set-up (with the exception of the fly-bar paddles, which are shown, but not included in the testing). The rotor bats are long thin circular cylinders. Three different lengths of rotor bats were tested, to assess the influence of torque-loading on motor/drive-train efficiency. A series of speed sweeps were conducted with the rotor bats. The results of the rotor bat tests, for one of the electric motors used during the MRC testing, is shown in Fig. 22.

Fig. 21 – Rotor Bats (with Fly-Bar paddles that were removed during testing)

Rotor bat and bare-shaft tests were conducted again to obtain power corrections for motor efficiencies of the new motor. A direct subtraction was made for the bare shaft tare for each separate RPM tested. The amount subtracted was dependent on the RPM tested. It was determined from rotor bat tests that the motor efficiency was essentially constant in the 800-1000 RPM range, independent of the load being applied to the motor.

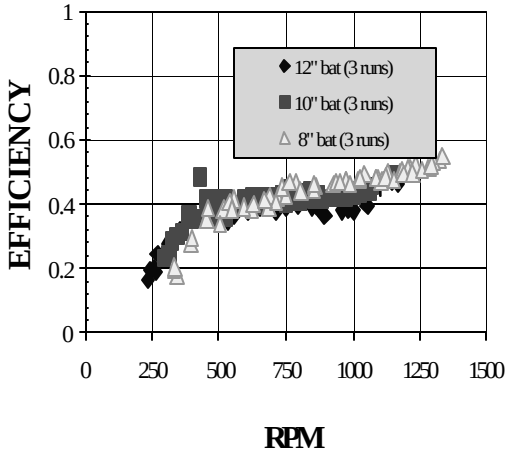

Fig. 22 – Rotor Bat Motor Efficiency Estimates for Three Rotor Bat Sets

Two conclusions were drawn from the rotor bat data. First, for the three rotor bats used during the test, little if any effect of torque loading was observed on the test-stand motor/drive-train efficiencies. Second, there was a speed dependency of the motor/drive-train efficiency observed in the rotor bat data. However, for the speed range of interest (800-1100 RPM) the efficiency curve was relatively flat. (As an aside, the rotor bat data pointed to a common problem with MAV, MRC, and electric hobbyist helicopters: that motor/drive-train efficiencies are far from being optimally tuned in terms of electromechanical performance for their particular applications.)

Alternatively, a small Prony brake apparatus was developed and used to test the electric motors used in the MRC hover test stand. A Prony brake relies upon dynamic friction from a clamp applied to the output shaft to torque-load a motor. A digital scale, with a lever and knife-edge combination resisting the motor torque, was used to measure the torque loading of the motor (Fig.23).

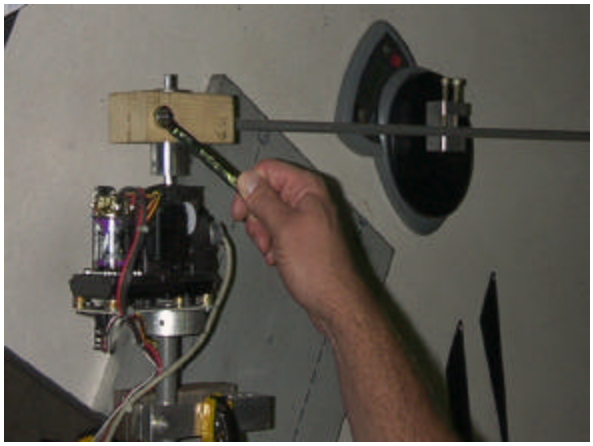

Fig. 23 – Prony Brake Set-Up

Representative results from the MRC motor/drive train efficiency testing are shown in Fig. 24 for nominal speeds of 800, 900, and 1000 RPM. As anticipated from the rotor bat data, there was not a significant torque-loading influence on the MRC hover test stand motor/drive-train efficiency.

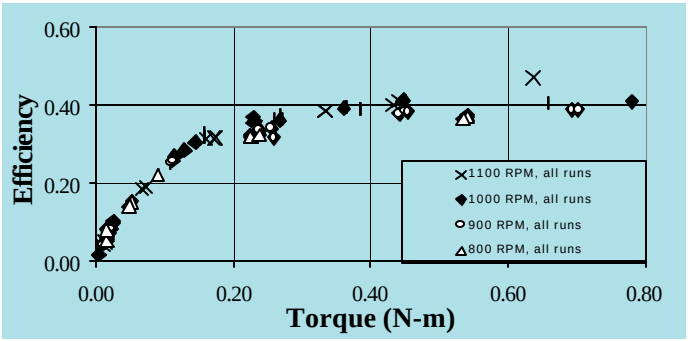

Fig. 24 – Representative Prony Brake Results

As can be seen in both Figs. 22 and 24 there is little speed sensitivity to hover test stand motor/drive-train efficiency in the range of 800-1100 RPM. There is an influence of torque loading on the motor/drive-train, but primarily at lower load levels. The following correction methodology has been implemented for the rotor performance measurements reported in this paper:

$$P = P_{Input}\, f\left(\frac{P_{Input}}{\Omega}\right) - P_{HT_{Input}}\, f\left(\frac{P_{HT_{Input}}}{\Omega}\right) \tag{1}$$

where P is the rotor shaft power corrected for hub tares (all data in the paper have hub tares applied), P_{Input} is the motor/drive-train input (electrical) power at the rotor test condition, $P_{HT\,Input}$ is the hub tare input (electrical) power. The form of the efficiency function, *f*, is derived from regression analysis of the Prony brake data of Fig. 24.

$$\eta_{em} = f(Q) = C_1 Q^{C_2} \tag{2}$$

Where, when Q is in N-m, C_1 = 0.486 and C_2=0.31 for the electric motors and drive-train used during the MRC rotor testing reported in this paper.